

## Chaotic Bouncing of a Droplet on a Soap Film

T. Gilet<sup>1,\*</sup> and John W. M. Bush<sup>2,†</sup>

<sup>1</sup>GRASP, Department of Physics B5a, University of Liège, B-4000 Liège, Belgium

<sup>2</sup>Department of Mathematics, Massachusetts Institute of Technology, Cambridge, Massachusetts 02139, USA

(Received 9 June 2008; published 5 January 2009)

We examine the complex dynamics arising when a water droplet bounces on a horizontal soap film suspended on a vertically oscillating circular frame. A variety of simple and complex periodic bouncing states are observed, in addition to multiperiodicity and period-doubling transitions to chaos. The system is simply and accurately modeled by a single ordinary differential equation, the numerical solution of which captures all the essential features of the observed behavior. Iterative maps and bifurcation diagrams indicate that the system exhibits all the features of a classic low-dimensional chaotic oscillator.

DOI: 10.1103/PhysRevLett.102.014501

PACS numbers: 47.55.D-, 47.52.+j

Couder *et al.* [1] have recently shown that oil droplets, when placed on a vertically vibrated oil bath, may bounce indefinitely rather than coalescing. The dynamics of the bouncing droplets are extraordinarily rich. Feedback between the droplet and its wave field may lead to self-propulsion [2] and diffraction of these walking droplets as they pass through a slit [3]; moreover, multiple droplets may lock into complex orbital motions [2] or lattices [4]. We here demonstrate that a droplet on a vertically vibrated soap film may similarly avoid coalescence, and that the bouncing droplet represents a textbook example of a chaotic oscillator, with many features common to the bouncing of an inelastic ball on a solid substrate.

Drops of uniform size ( $R = 0.08$  cm) bounce on a horizontal circular soap film of radius  $A = 1.6$  cm vibrated with vertical displacement  $B \cos(2\pi ft)$  (Fig. 1). The droplet and soap film consist of a glycerol-water-soap mixture (80% water, 20% glycerol, <1% soap) with density  $\rho = 1.05$  g cm<sup>-3</sup>, viscosity  $\nu = 2$  cS, and surface tension  $\sigma = 22$  dyn cm<sup>-1</sup>. Drops of uniform size ( $R = 0.8$  mm) and mass ( $m = 2.25$  mg) were extruded from an insulin syringe (needle diameter 0.35 mm). For the bouncing states, the characteristic drop impact speeds ( $U \sim 4\text{--}32$  cm s<sup>-1</sup>) are much less than the characteristic wave speed on the film (a film thickness of  $4$   $\mu$ m indicates a wave speed of  $\sqrt{2\sigma/\rho h} \sim 330$  cm s<sup>-1</sup>). The influence of capillary waves is thus assumed to be negligible, and the film described as quasistatic: it deforms instantaneously in response to the forcing imposed by the droplet. The Weber number  $We = \rho U^2 R / \sigma$  lies between 0.06 and 3.9. During impact, the droplet remains roughly spherical: maximum center line distortions of 13% were observed (at  $We = 3.9$ ), so the surface energy of drop distortion is less than 3% that associated with soap film distortion. Beneath the droplet, the soap film lies tangent to the droplet, and so roughly assumes the form of a spherical cap of radius  $R$ . Beyond the droplet, the pressure is atmospheric on either side of the soap film, which thus assumes the form of a catenoid as confirmed experimentally [5]. The spherical cap and catenoid

match at a point  $M$  corresponding to an angle  $\alpha$  (Fig. 1). The vertical deflection of the soap film  $Z$  and the resulting vertical force  $F$  on the droplet may be expressed in terms of  $\alpha$ :

$$\frac{Z}{R} = 1 - \cos\alpha + \sin^2\alpha \ln\left[\frac{\tan\frac{\alpha}{2}}{\beta}(1 + \sqrt{1 - \beta^2})\right], \quad (1)$$

$$F = 4\pi\sigma R \sin^2\alpha,$$

where  $\beta = (R \sin^2\alpha)/A$ . The force-displacement relation  $F(Z)$  is shown in Fig. 2(a). In the range  $0 < Z/R < 3$ , the film responds as a linear spring,  $F = kZ$ , where the effective spring constant  $k = \frac{8\pi}{7}\sigma$ . The force then saturates, achieving a maximum at  $\alpha = \pi/2$ , and decreases thereafter. This quasistatic description of the film was used successfully by the authors [5] to deduce a criterion for breakthrough of a droplet striking a stationary film [6].

When the droplet strikes a static soap film at a speed  $U$ , the drop is in apparent contact with the film for a time  $t_c$ . Dissipation during rebound results in the kinetic energy at takeoff being less than that at impact. Figure 2(b) illustrates the dependence of the dimensionless contact time  $\tau_c = t_c/\tau_\sigma$  and dissipated energy  $\Delta(V^2/2)$  on the dimen-

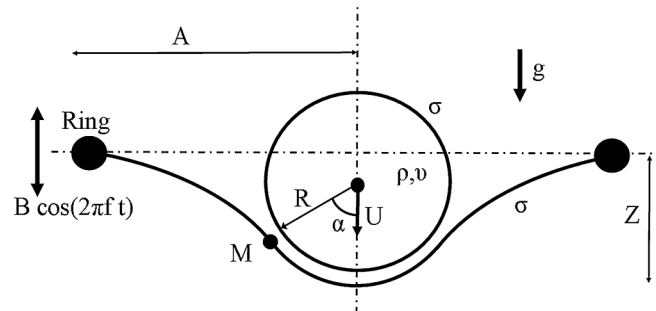


FIG. 1. Experimental system: a droplet of radius  $R = 0.08$  cm bounces on a soap film of radius  $A = 1.6$  cm vibrated with vertical displacement  $B \cos 2\pi ft$ . The soap film assumes the form of a spherical cap beneath the droplet, and a catenoid beyond the matching point  $M$ .

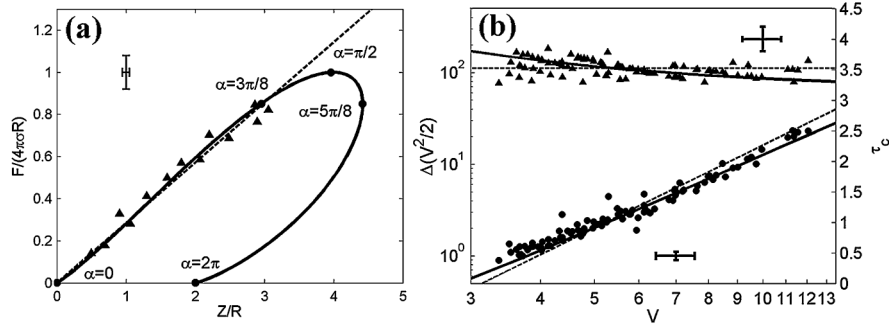


FIG. 2. (a) Relation between the maximum soap film deflection  $Z$  and the resulting vertical force  $F$  acting on the droplet. Triangles represent experimental measurements inferred from droplet trajectories. The solid line corresponds to the force anticipated on the basis of our theoretical approximation of the soap film shape (1). The dashed line is the linear approximation  $F = 8\pi\sigma Z/7$ , valid for  $Z/R < 3$ . (b) Left axis, solid circles: Energy dissipated,  $\Delta(V^2/2)$ , during impact on a static soap film as a function of the dimensionless impact speed  $V = U/(g\tau_\sigma)$ . The dashed line is the best-fit  $\Delta(V^2/2) = 0.016V^3$ . Right axis, triangles: Contact time  $\tau_c = t_c/\tau_\sigma$  as a function of the impact speed  $V$ . The dashed line is the best-fit law  $\tau_c = 3.52$ . The solid lines correspond to the numerical solution of Eq. (2) with  $\Gamma = 0$  and  $\Psi = 0.01$ . Characteristic error bars are shown.

dimensionless impact speed  $V = U/(g\tau_\sigma)$ , where  $\tau_\sigma = \sqrt{m/k}$  and  $g$  is the gravitational acceleration. Note that the contact time is independent of the impact speed  $V$  and proportional to  $\tau_c$ , as is consistent with the film behaving as a linear spring, and as was observed for droplets bouncing on hydrophobic substrates [7]. The dissipated energy increases as  $V^3$ , a scaling that we shall exploit in our theoretical modeling.

On a sinusoidally forced soap film, periodic bouncing occurs in the range where the soap film behaves as a linear spring (Fig. 3). The droplet trajectory is prescribed by a force balance: the drop accelerates in response to gravity and the force applied by the soap film, the latter of which acts only when the drop is in apparent contact with the film. A dissipative force proportional to  $kU^2/g$  accounts for the dissipated energy, which grows as  $V^3$ . Writing the force balance in the accelerating reference frame of the bounding ring introduces a sinusoidal forcing term. In dimensionless form, the force balance thus assumes the form

$$\frac{d^2y}{d\tau^2} = -H(-y)y - 1 - \Psi H(-y)|\dot{y}| \dot{y} + \Gamma \cos(\omega\tau + \phi), \quad (2)$$

where  $\tau = t/\tau_\sigma$ ,  $y = -Z/(g\tau_\sigma^2)$ ,  $\Gamma = 4\pi^2 Bf^2/g$ ,  $\omega = 2\pi f\tau_\sigma$ , and  $H(y)$  is the Heaviside function. The coefficient  $\Psi = 0.01$  is inferred from the experimental data reported in Fig. 2(b). In many respects, the numerical solution of Eq. (2) yields remarkably good agreement with the experimental data. In Fig. 4(a), we demonstrate the excellent agreement between the observed trajectory of a drop released above an unforced film and that predicted by Eq. (2) for  $\Gamma = 0$ .

The film forcing provides energy to the droplet. If this energy precisely balances that lost through dissipation during impact, the droplet executes a periodic bouncing motion. We denote by  $(m, n)$  a periodic state in which the

droplet bounces  $n$  times and the soap film oscillates  $m$  times during a single period. A myriad of simple ( $n = 1$ ) and complex ( $n > 1$ ) periodic states were observed experimentally, including (1, 1), (2, 1), (3, 1), (3, 3), and (2, 2) (Fig. 3). Mode transitions characterized by either aperiodic transients or period-doubling cascades were observed as the forcing parameters were varied (see supplementary material in Ref. [8]). Multiperiodicity is apparent in Figs. 3(a)–3(c): multiple periodic solutions (1, 1), (2, 1), and (3, 1) arise for precisely the same forcing parameters  $(\omega, \Gamma) = (0.6, 1.1)$ , but different initial conditions. With  $\omega = 0.6$  fixed, complex periodic states were apparent at higher  $\Gamma$  [Figs. 3(d) and 3(e)], and ultimately chaos emerges for  $\Gamma \geq 1.1$  [Fig. 3(f)]. As seen in Figs. 4(b) and 4(c), the computed periodic solutions of Eq. (2) are remarkably close to those observed experimentally; in particular, the landing and takeoff phases are in good agreement. As a caveat, we note that complex modes ( $m$ ,

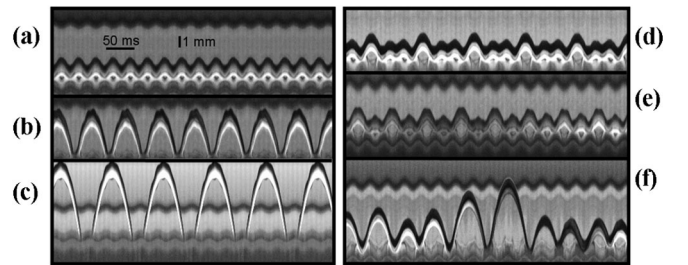


FIG. 3. Spatiotemporal diagrams of bouncing states observed experimentally at  $\omega = 1.1$  ( $f = 33$  Hz). The images are formed by compiling side-by-side vertical center line columns of successive video images: time is represented by the horizontal coordinate. For a periodic bouncing state denoted by  $(m, n)$ , the droplet bounces  $n$  times, while the soap film oscillates  $m$  times. (a) Mode (1, 1) at  $\Gamma = 0.6$ . (b) Mode (2, 1) at  $\Gamma = 0.6$ . (c) Mode (3, 1) at  $\Gamma = 0.6$ . (d) Mode (3, 3) at  $\Gamma = 0.7$ . (e) Mode (2, 2) at  $\Gamma = 1.2$ . (f) Chaotic motion at  $\Gamma = 1.1$ .

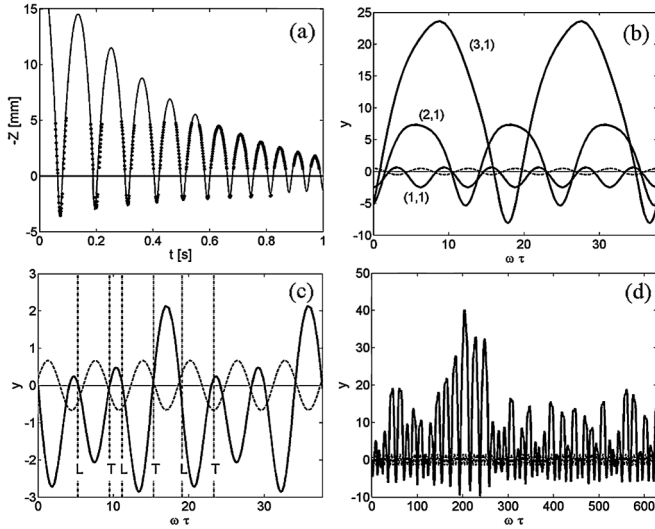


FIG. 4. Numerical solutions of Eq. (2) at  $\omega = 1.1$  with a coefficient of dissipation  $\Psi = 0.01$  inferred from Fig. 2(b). (a) Observed (dots) and simulated (solid line) trajectories of a droplet bouncing on a stationary soap film ( $\Gamma = 0$ ). (b) Modes (1, 1), (2, 1), and (3, 1) at  $\Gamma = 0.6$ . (c) Mode (3, 3) at  $\Gamma = 0.82$ . The landing and takeoff phases measured experimentally are represented by vertical lines denoted by  $L$  and  $T$ , respectively. (d) Chaotic motion at  $\Gamma = 2$ . In (b-c), the dashed line indicates the ring motion.

$n > 1$ ) and the onset of chaotic motion are observed at slightly lower accelerations in the experiments than the numerics.

Solutions of Eq. (2) may be displayed on a Poincaré section by computing the speed and phase at impact,  $(y, \dot{y}) = (0, -V)$ . Equation (2) is integrated numerically from one impact to the next, for various initial conditions  $(V, \phi)$ . A two-dimensional iterative map may thus be defined as

$$V_{i+1} = f(V_i, \phi_i), \quad \phi_{i+1} = g(V_i, \phi_i). \quad (3)$$

Poincaré sections are represented in Figs. 5(a) and 5(b) for  $\Gamma = 0.82$  and  $\Gamma = 1.82$ , respectively. For each set of initial conditions  $(V_i, \phi_i)$ , contours of the net energy acquired by the drop during impact,  $V_{i+1}^2 - V_i^2$ , are computed. The shaded area corresponds to initial conditions for which energy is gained during impact; in the white area, energy is lost. Simple modes  $(m, 1)$  are represented by single points that necessarily lie on the boundary of the shaded area: no energy is gained or lost during impact, so the bouncing is perfectly periodic over a single forcing cycle. Complex modes  $(m, n > 1)$  are represented by closed curves that cross the zero-energy boundary. For example, in the (3, 3) mode [Figs. 3(d) and 5(a)], energy is transferred to the droplet during the first two impacts, increasing the leap height; however, during the third bounce, energy is lost and the initial conditions are recovered. At  $\Gamma = 1.82$ , the motion is chaotic, and a strange attractor emerges on the Poincaré section [Fig. 5(b)]. (See supplementary material in Ref. [8] for a Smale map diagnostic.)

A bifurcation diagram [Fig. 6(a)] represents the solution of Eq. (2) as a function of  $\Gamma$  for  $\omega = 1.1$ . For  $\Gamma < 0.17$ , no periodic bouncing states are possible: the droplet resides at rest on the soap film. The first periodic solution (2, 1) appears at  $\Gamma = 0.17$ . As  $\Gamma$  is progressively increased, simple modes  $(m, 1)$  and complex modes  $(m, n)$  appear in turn. At branch points, modes  $(m, n)$  execute a period-doubling transition to a  $(2m, 2n)$  mode. For example, the mode (2, 1) gives rise to a period-doubling cascade that terminates at  $\Gamma \approx 1.67$  [Fig. 6(b)]. Thereafter, the complex periodic modes degenerate into a strange attractor that may coexist with stable periodic orbits emerging from other branches [shaded area in Fig. 6(a)]. For  $\Gamma > 1.91$ , no such periodic branches persist, and the chaotic attractor is the only attracting set.

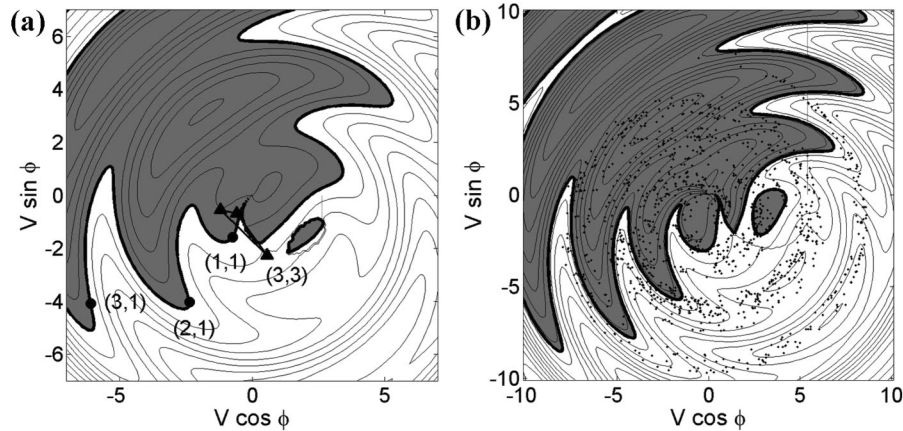


FIG. 5. Iterative maps  $(V, \phi)$  in polar coordinates. Curves represent contours of energy transferred to the droplet,  $V_{i+1}^2 - V_i^2$ , as a function of impact speed  $V$  and phase  $\phi$ , at  $\omega = 1.1$ . The droplet gains and loses energy when it impacts in, respectively, the shaded and white regions. (a)  $\Gamma = 0.82$ : The filled circles represent simple periodic modes  $(m, 1)$ , and the triangles, complex periodic mode (3, 3). Contours are spaced by  $\Delta(V^2) = 2$ . (b) Chaotic solutions at  $\Gamma = 1.82$ . The dots correspond to the Poincaré section of a spiraling strange attractor. Contours are spaced by  $\Delta(V^2) = 5$ .

